Corrosion Resistance of Fe-Based Bulk Amorphous Alloy with Sulfide Inclusion

Y. Zuo, S. L. Wang, Y. Huang and S. X. Wang

Abstract Corrosion resistance of Fe-based bulk metallic glass with sulfide inclusion was investigated in HCl, H_2SO_4, NaCl and NaOH solutions at different ambient temperature. The results indicate that Fe-based amorphous alloy generally exhibits more excellent corrosion resistance in alkaline solutions than that in acidic solutions, and presents high spontaneous passivated ability and evident passivation region in all solutions. Electrochemical impedance spectroscopy results display that all of the Nyquist curves are composed of just a single capacitive loop, and the electrode reaction is mainly controlled by the electrode potential. The mass loss exceeds 0.67 mg/cm^2 in 0.5 M H_2SO_4 solution, and rapider than that in another solutions. With increase of ambient temperature, the corrosion resistance decreases in all solutions. No pitting corrosion occurs in acidic solutions, though the inclusion particle is dissolved firstly. Seemly, some pit can be formed in NaCl solution, when ambient temperature exceeds 60 °C.

Keywords Fe-based bulk metallic glass · Sulfide · Pitting corrosion
Ambient temperature

Introduction

Due to excellent corrosion resistance and high microhardness, Fe-based amorphous alloys present an extensive potential application as anti-corrosive or anti-wearing materials, such as nuclear power, thermal power, ship, automobile, sports equipment, and so on. So many Fe-base amorphous alloy systems as Fe–Co–B–Si–Nb–Cr [1], Fe–Co–Cr–Mo–C–B–Y [2], Fe–Cr–Mo–C–B [3], Fe–Si–B–Nb–Cu [4], have been developed in the last decades. Since the high brittleness, Farmaer et al. [5] has attempted the applications of Fe-based amorphous coatings on the

Y. Zuo · S. L. Wang (✉) · Y. Huang · S. X. Wang
National Defence Key Disciplines Laboratory of Light Alloy Processing Science and Technology, Nanchang Hangkong University, Nanchang 330063, Jiangxi, China
e-mail: slwang70518@nchu.edu.cn

Y. Han (ed.), *Advanced Functional Materials*,
https://doi.org/10.1007/978-981-13-0110-0_35

containers for the transportation, aging and disposal of spent nuclear fuel. The neutron absorption cross section in transmission for thermal neutrons of $Fe_{49.7}Cr_{17.7}Mn_{1.9}Mo_{7.4}W_{1.6}B_{15.2}C_{3.8}Si_{2.4}$ (SAM2X5) with high boron content is four times greater than that of borated stainless steel, and twice as good as nickel-based alloy (C-4) with additions of Gd. The Fe-based amorphous coating with the composition of $Fe_{54.2}Cr_{18.3}Mo_{13.7}Mn_2W_6B_{3.3}C_{1.1}Si_{1.4}$(wt%) on the marine pump impellers exhibits 2–3 times erosion rate than that of SUS304, believed to enhance effectively the lifetime of pump impellers in sand-containing seawater [6]. The corrosion rate of Fe-based amorphous coating of $Fe_{48}Cr_{16}Mo_{16}C_{14}B_2Mn_2Y_2$ is 1/1000 of that of 20G steel in the artificial simulation environment of power plant Boiler [7]. However, for all Fe-based amorphous alloys above mentioned, the produce cost is very high since high pure elements, which limits the extensive application in industries.

In our group, the Fe–C–Si–B–P–Cr–(Mo, Al, Co) amorphous alloy was developed using cast iron, industrial ferroalloys and commercial grade elements [8, 9]. Effects of elements, pH, ambient temperature on corrosion resistance were investigated in the published literatures [10, 11]. Since the impurity elements of oxygen and sulphur in raw materials, some oxide and sulphide can be detected in some bulk amorphous alloy. The effect of sulphur on the glass forming ability and corrosion resistance was investigated [12, 13]. However, effect of sulphide on corrosion behaviors of Fe-based amorphous alloy is unknown. In this paper, the corrosion resistance of Fe-based bulk amorphous alloy with sulphide inclusion will be discussed in difference solutions.

Experimental

The Fe-based amorphous alloy rods with the nominal composition of $Fe_{66.6}C_{7.1}Si_{3.3}B_{5.5}P_{8.7}Cr_{2.3}Mo_{2.5}Al_{2.0}Co_{1.0}S_{1.0}$ (at.%) were fabricated by the water cooling copper mold suction-casting, and the detailed processing and the composition of raw materials were shown in the literature [9]. Prior to immersion tests and electrochemical measurements, the specimens were degreased in acetone, washed in distilled water and dried in air. Corrosion rates were estimated from the weight loss after immersed in 0.5 M HCl, H_2SO_4, NaCl and NaOH solutions, respectively, open to air at room temperature for 30 days. The electrochemical measurements were conducted by a potentiostat (CHI 660E PARSTAT) and a three-electrode cell. The counter electrode was platinum and the reference electrode was a saturated calomel electrode (SCE). The potentiodynamic polarizations were measured in 1 M HCl, H_2SO_4, NaCl and NaOH solutions with 60 mV/min sweep rate at 20, 40 and 60 °C, respectively. The potentiostatic polarization were conducted by applying a potential of 0.5 V in acidic solutions or 0 V (SCE) in alkaline solutions for 2 h at different ambient temperatures. The electrochemical impedance was measured from 0.01 Hz to 100 kHz with the AC mode after the specimens were immersed for

20 min to obtain a stable open circuit potential. After immersion, the surface morphologies were observed by scanning electron microscope (SEM).

Results and Discussions

Figure 1 shows the potentiodynamic polarization curves in 1 M HCl, H_2SO_4, NaCl and NaOH solutions at different ambient temperature. In HCl solution, the specimen exhibits spontaneous passivation when scanning voltage exceeds 0.3 V, and presents transpassivation as scanning voltage is larger than 1.2 V in different ambient temperature. As the ambient temperature increases, corrosion current density and passive current density also increases, while corrosion potential and passive potential region seem no variation. The all related electrochemical results are shown in Table 1. Compared with HCl solution, a similar tendency can been attained in 1 M H_2SO_4, NaCl and NaOH solutions.

The current density versus passivation time during the potentiostatic polarization in four solutions is shown in Fig. 2. The applied potential of 0.5 V was selected

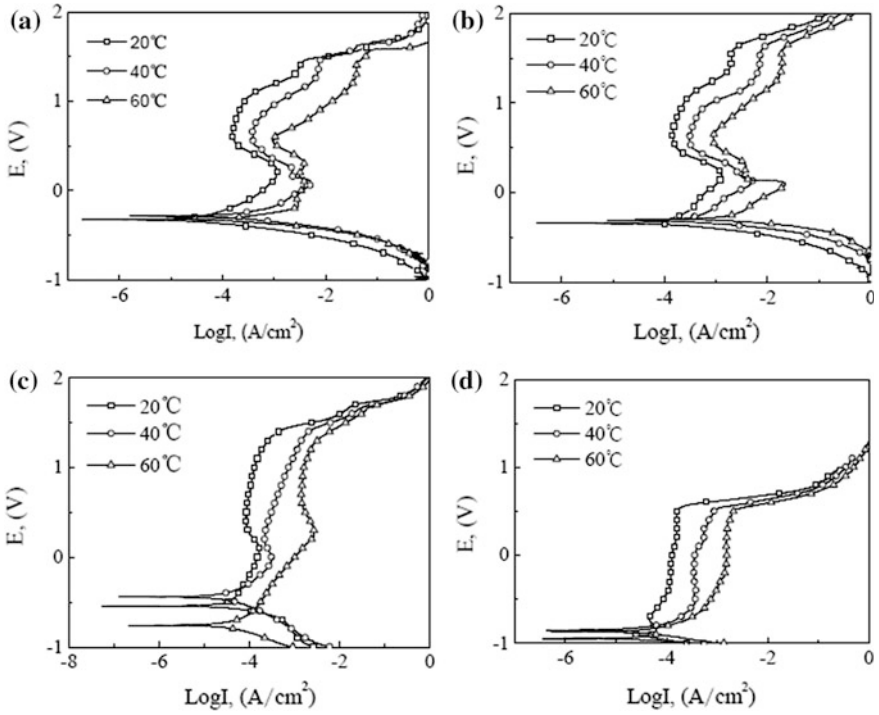

Fig. 1 Potentiodynamic polarization in difference solutions, **a** HCl, **b** H_2SO_4, **c** NaCl and **d** NaOH

Table 1 The results obtained from electrochemical tests

Solutions	Temperature (°C)	I_{corr} (μA/cm^2)	I_{pass} (μA/cm^2)	E_{corr} (−V)	E_{pit}−E_{pass}	CPE (μA/cm^2)	R_P (Ω/cm^2)
HCl	20	33.9	154.9	0.32	1.24	25.ro2	28,209
	40	111.2	382.8	0.28	1.21	108.3	6169
	60	125.3	955.0	0.32	1.13	499.4	734
	20	66.1	135.8	0.33	1.44	9.8	115,690
H_2SO_4	40	232.0	300.1	0.31	1.51	51.6	9925
	60	461.6	598.4	0.29	1.56	315.1	1104
	20	46.8	104.7	0.54	1.30	2.3	12,365
NaCl	40	50.1	489.8	0.43	1.43	2.9	30,673
	60	79.4	1013.6	0.75	1.0	5.3	10,290
	20	12.2	131.8	0.94	1.41	0.7	8589
NaOH	40	16.5	182.0	0.90	1.03	1.0	2613
	60	29.0	208.9	0.91	1.01	7.43	1293

from the potentiodynamic polarization curves. In HCl solution, the current densities decrease continuously with time and finally reach a steady state current density at 20 °C. While as ambient temperature exceeds 40 °C, the potentiostatic polarization curves are different. Corrosion current density decreases to near 30 μA/cm^2 during first 200 s, and then increases sharply, finally reaches a steady state current density of 700 μA/cm^2 in the 40 °C. As ambient temperature reaches 60 °C, corrosion current density decreases during first 500 s, the lowest current density is near 200 μA/cm^2. And then it increases sharply, finally reaches a steady state current density of 950 μA/cm^2. Only when ambient temperature exceeds 60 °C, the corrosion current density decreases firstly, and then increases, finally reaches a steady state in H_2SO_4 solution. While in NaCl solution, the current density can't reach a steady state, and increase gradually as increase of time at 60 °C. Moreover, many peak of corrosion current density increasing can be observed during scanning time at 60 °C, which means pitting corrosion. Though ambient temperature exceeds 60 °C, the current densities decrease continuously with time and finally reach a steady state current density in NaOH solution.

Figure 3 shows Nyquist polts obtained from electrochemical impedance spectroscopy measurements in different solutions. The experimental data in the figure are presented as symbols and the solid lines are attained by curve fitting using non-linear-least-square fit analysis [10]. The charge transfer resistance decreases continuously with increase of ambient temperature in all solution. The opposite behavior is observed for the capacitance, as shown in Table 1.

Figure 4 presents the mass loss with the immersion time. It can be observed mass loss increases during the first stage, and then reaches a steady state in four solutions. The highest mass loss rate exceeds 0.67 mg/cm^2 in H_2SO_4 solution, the lowest mass loss rate is near to 0.04 mg/cm^2 in NaCl solution. During immersion

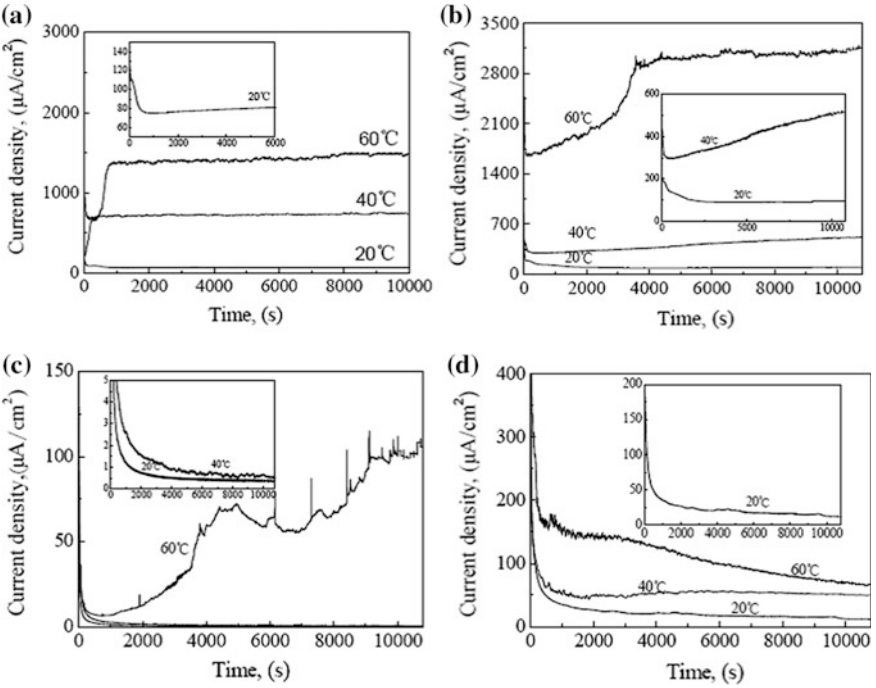

Fig. 2 Potentiostatic polarization in difference solutions, **a** HCl, **b** H_2SO_4, **c** NaCl and **d** NaOH

test, as no passive film is formed on the surface, the mass loss increases with time at first stage. The mass loss is stable gradually, since the formation of passive film and the precipitation of corrosion products on the surface with immersion time increase.

The surface morphologies immersed in four solutions are shown in Figs. 5, 6, 7 and 8. The 'dried riverbed' cracked morphologies are clearly observed on the surface immersed in acidic solutions, as shown in Fig. 5 (HCl solution) and Fig. 6 (H_2SO_4 solution). While no crack, just smoothing surfaces are remained in NaCl (Fig. 7) and NaOH (Fig. 8) solutions. In acidic solutions, firstly, the groove is observed near the inclusion particle in Fig. 5b, and then some cracks originate from the inclusion particles, even pass through them, as shown in Figs. 5c and 6b. Finally, more and more cracks are formed and propagated along all direction on the surface, thus the 'dried riverbed' cracked morphologies are formed, as shown in Figs. 5d and 6d. According to the variety of corrosion morphology characteristics, it may be deduced that the inclusion particles are dissolved firstly, and some corrosion products are formed on the position of inclusion particles. With acceleration of corrosion products on the surface, the microstructure in the position of inclusion particles becomes more loosing, compared to other. Therefore, the cracks will initiate and propagate with the great internal stress in the cast specimen.

In alkaline solutions, it is well know that Fe_2O_3 is main corrosion product and it is stable. So a greater amount of Fe_2O_3 will precipitated on the surface and this was

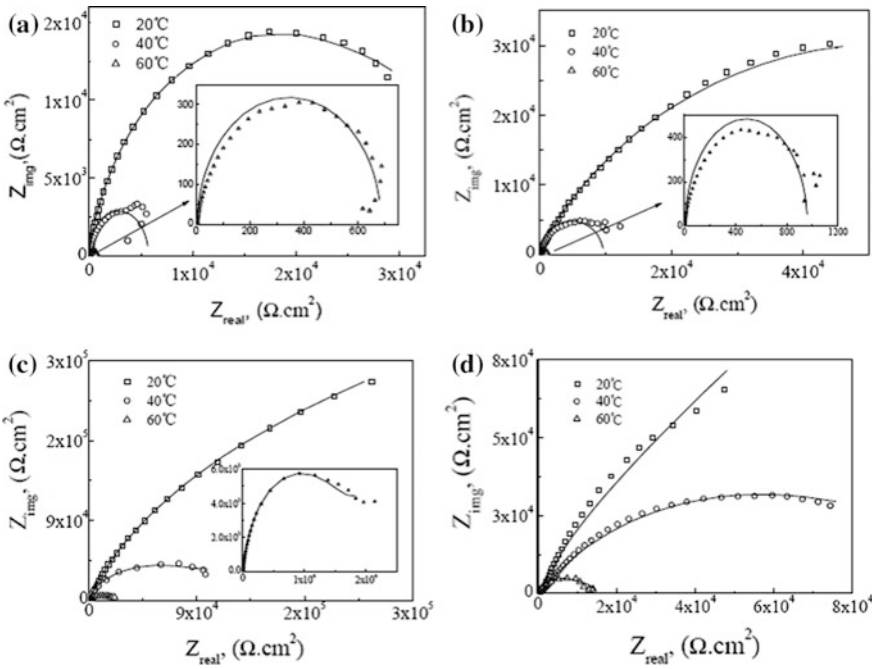

Fig. 3 Nyquist plots n in difference solutions, **a** HCl, **b** H_2SO_4, **c** NaCl and **d** NaOH

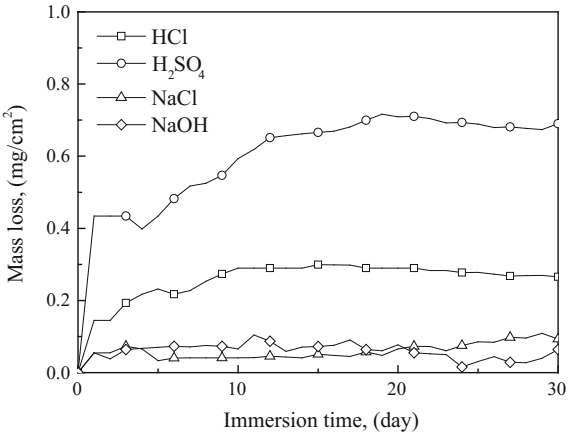

Fig. 4 Corrosion rate in difference solution at room temperature

indentified in the literature [10]. The acicular shape Fe_2O_3 layer is porosity and loosing, which is benefit to the release of internal stress in cast specimen. Therefore, no crack is formed on the surface.

It is well known that the reaction rate is accelerated generally since the intensifying activity of ions or elements with increase of ambient temperature. Though

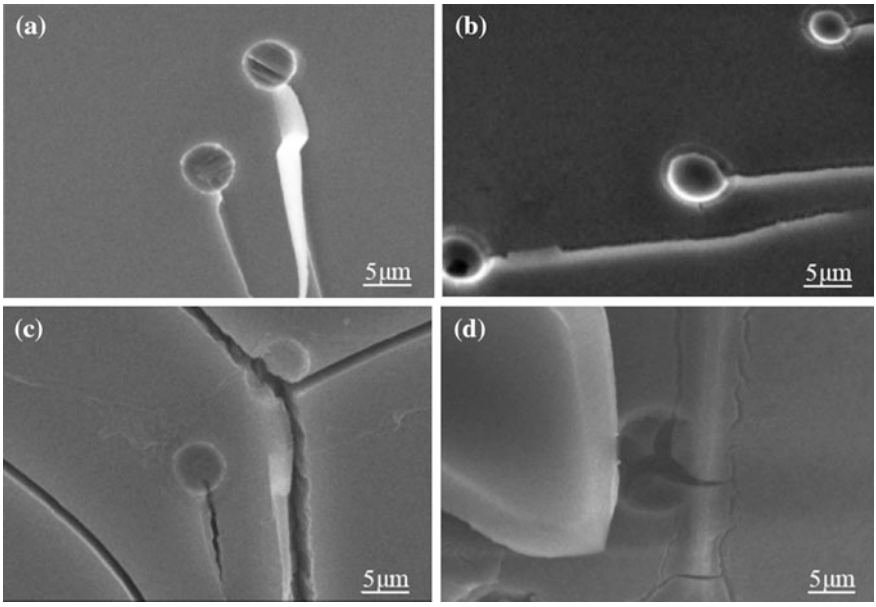

Fig. 5 Corrosive surface morphology in 0.5 M HCl solution, **a** as-cast, **b** 1 day, **c** 3 days and **d** 7 days

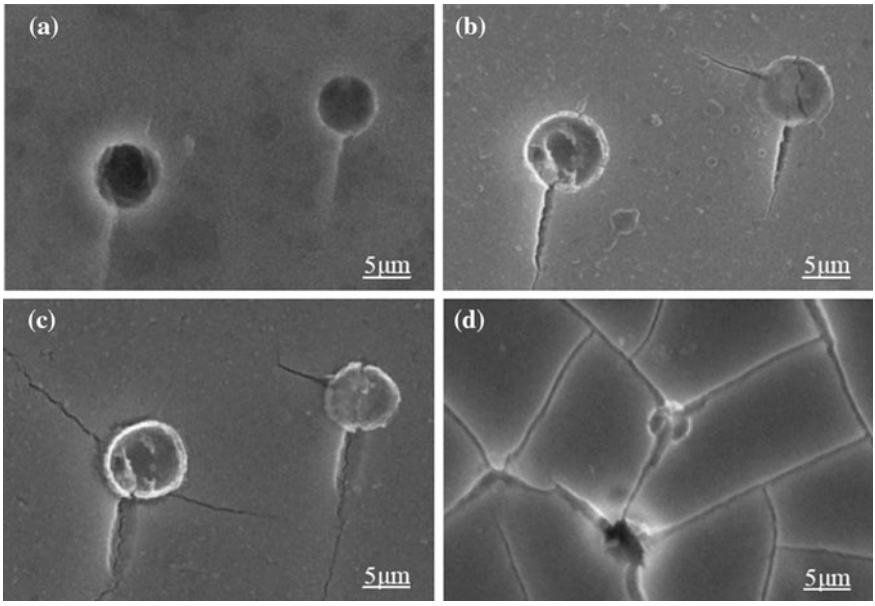

Fig. 6 Corrosive surface morphology in 0.5 M H_2SO_4 solution, **a** as-cast, **b** 1 day, **c** 3 days and **d** 7 days

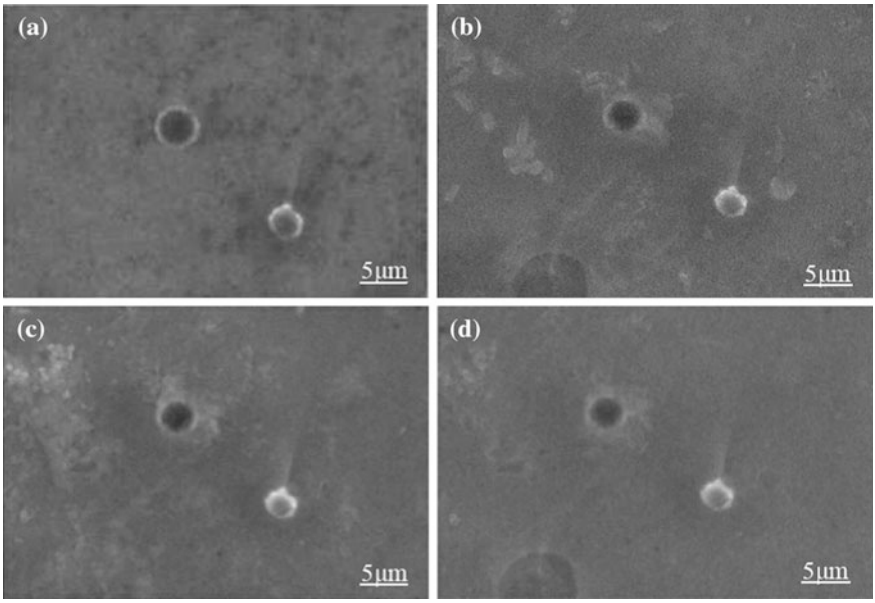

Fig. 7 Corrosive surface morphology in 0.5 M NaCl solution, **a** as-cast, **b** 1 day, **c** 3 days and **d** 7 days

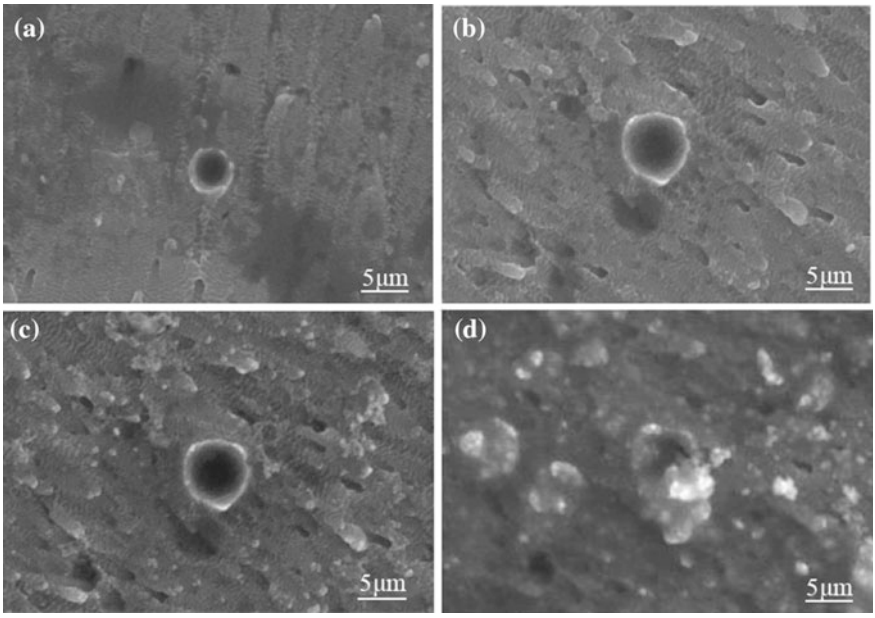

Fig. 8 Corrosive surface morphology in 0.5 M NaOH solution, **a** as-cast, **b** 1 day, **c** 3 days and **d** 7 days

$Fe_{48.7}Cr_{18}Mn_{1.9}Mo_{7.4}W_{1.6}V_{15.2}C_{3.8}Si_{2.4}$ amorphous alloy coating is spontaneously passivated with a low passive current density in different ambient temperatures, the passive current density progressively increases and the pitting potential decreases as temperature increases [14]. While the erosion rates of FeBSiNb amorphous coating decrease with increase of test temperature, since the formation of a thick oxide, and surface characteristic modification during erosion testing [15]. Liu [16] found that the Fe-based amorphous composite exhibits an excellent hot corrosion resistance and excellent thermal stability in molten Na_2SO_4 + K_2SO_4 salt at 923 K, due to the formation of a continuous and protective Cr_2O_3 oxide which acts as an effective barrier to the inward diffusion of corrosive species during the hot corrosion process.

In general, the CPE is related to the layer capacitance of the electrode. The thicker the corrosion product is, the higher the CPE is. With increase of ambient temperature, the corrosion reaction is also accelerating, thus the corrosion product is accumulating. The R_{ct} is charge transfer resistance. The increase of R_{ct} indicates an increase in the insulating character of the oxide film [17].

Conclusions

(1) With increase of ambient temperature, the corrosion rate of Fe-based amorphous alloy will accelerate in all solutions.
(2) No pitting corrosion occurs in acidic solutions, though the inclusion particle is dissolved firstly. Seemly, some pit can be formed in NaCl solution, when ambient temperature exceeds 60 °C.
(3) Fe-based amorphous alloy generally exhibits more excellent corrosion resistance in alkaline solutions than that in acidic solutions.

Acknowledgements The work was supported by the National Natural Science Foundation of China (No. 51461031), Department of Education Fund of Jiangxi Province (GJJ150733), Natural Science Foundation of Jiangxi Province (20161BBH80031) and Power Construction Corporation of China (DJ-ZDXM-2014-34).

References

1. Z.L. Long, Y. Shao, A. Inoue, Cr effects on magnetic and corrosion properties of Fe–Co–Si–B–Nb–Cr bulk glassy alloys with high glass-forming ability. Intermetallics **15**, 1453–1458 (2007)
2. H.B. Fan, W. Zhang, J. Shen, Corrosion behavior of $Fe_{41}Co_7Cr_{15}Mo_{14}C_{15}B_6Y_2$ bulk metallic glass in sulfuric acid solutions. Metallur. Mater. Trans. A **42**, 1524–1533 (2011)
3. S.J. Pang, T. Zhang, A. Inoue, Bulk glassy Fe–Cr–Mo–C–B alloys with high corrosion resistance. Corr. Sci. **44**, 1847–1856 (2002)

4. A. Pardo, E. Otero, M.C. Merino, Influence of Cr addition on the corrosion resistance and magnetic properties of amorphous $Fe_{73.5}Si_{13.5}B_9Nb_3Cu_1$ in simulated industrial environments. J. Non-Cryst. Solids **287**, 421–427 (2001)
5. J.C. Farmer, J. Haslam, S. Day, The corrosion resistance of Fe-based amorphous metals: $Fe_{49.7}Cr_{17.7}Mn_{1.9}Mo_{7.4}W_{1.6}B_{15.2}C_{3.8}Si_{2.4}$ and other compositions. Mater. Sci. Tech. 318–392 (2007)
6. Y. Wang, Y.G. Zheng, Z.M. Yao, Investigation of HVOF-sprayed Fe-based amorphous metallic coatings with high erosion resistance and corrosion resistance, in *The 6th China Corrosion Conference*, pp. 1030–1036 (2011)
7. J. Lu, C. Liu, Y. Han, Analysis of utilizing anti-corrosion Fe-based amorphous coating material with the flue gas waste heat in the power plant boiler. Electr. Power Sci. Eng. **30**, 13–18 (2014)
8. H.X. Li, J.E. Gao, S.L. Wang, Formation, crystallization behavior, and soft magnetic properties of FeCSiBP bulk metallic glass fabricated using industrial raw materials. Metall. Mater. Trans. A **43A**, 2615–2619 (2012)
9. S.L. Wang, H.X. Li, S. Yi, Effects of Cr contents in Fe-based bulk metallic glasses on the glass forming ability and the corrosion resistance. Mater. Chem. Phys. **113**, 878–883 (2009)
10. S.L. Wang, H.X. Li, S. Yi, Effects of electrolyte pH on the electrochemical behavior of Fe-based bulk metallic glass. Met. Mater. Inter. **18**, 791–797 (2012)
11. S.L. Wang, S. Yi, The corrosion behaviors of Fe-based bulk metallic glasses in a sulfuric solution at 70 & #xB0;C. Intermetallics **18**, 1950–1953 (2010)
12. S.L. Wang, J.C. Cheng, S. Yi, Precipitation of sulfide particle in situ formed in Fe-based bulk metallic glass. Foundy **62**, 491–495 (2013)
13. S.L. Wang, S.B. Chen, S. Yi, Effects of sulphide on pit corrosion in metallic glass steel. Mater. Res. Innov. **18**, 638–641 (2014)
14. R.Q. Guo, C. Zhang, L. Liu, Corrosion and wear resistance of a Fe-based amorphous coating in underground environment. Intermetallics **30**, 94–99 (2011)
15. J.B. Cheng, X.B. Liang, Y.X. Chen, High-temperature erosion resistance of FeBSiNb amorphous coatings deposited by arc spraying for boiler applications. J. Therm. Spray. Techn. 820–827 (2013)
16. W.Y. Liu, Y. Hou, C. Liu, Hot corrosion behavior of a centimeter Fe-based amorphous composite coating prepared by laser cladding in molten Na_2SO_4 + K_2SO_4 salts. Surf. Coat. Techn. **270**, 33–38 (2015)
17. F. Rosalbino, S. Delsante, G. Borzone, Influence of rare earth metals on the characteristics of anodic oxide films on aluminium and their dissolution behaviour in NaOH solution. Corr. Sci. **52**, 322–328 (2010)